Cluster formation, waterlike anomalies, and re-entrant melting for a family of bounded repulsive interaction potentials

Erik Lascaris,[1] Gianpietro Malescio,[2] Sergey V. Buldyrev,[1,3] and H. Eugene Stanley[1]
[1]*Center for Polymer Studies and Department of Physics, Boston University, Boston, Massachusetts 02215, USA*
[2]*Dipartimento di Fisica, Università degli Studi di Messina, Contrada Papardo, 98166 Messina, Italy*
[3]*Department of Physics, Yeshiva University, 500 West 185th Street, New York, New York 10033, USA*
(Received 4 December 2009; published 22 March 2010)

We introduce a family of bounded repulsive potentials, which we call the cut ramp potential, obtained by cutting a linear ramp potential at different heights. We find that for the *uncut* ramp potential the system shows a region of anomalous re-entrant melting (a negative slope of the melting line in the temperature-pressure phase diagram), with waterlike anomalies in the same pressure range. At high pressure the melting line recovers a positive slope, a feature that we associate with the formation of clusters of particles separated by a more or less density-independent distance, the cluster separation, which is approximately equal to the ramp width σ_1. As the ramp is cut at lower and lower heights, the region of anomalous behavior shrinks and eventually disappears while at the same time the formation of clusters becomes more favored, as it is energetically less unfavorable for particles to "climb up" the ramp. We relate the occurrence of anomalous behavior to the reduced efficacy of the soft repulsive length scale with increasing pressure. The clustering phenomenon partially restores this efficacy, giving rise to an approximately constant distance σ_1 between the clusters. Our results may be useful to better understand the phase behavior of macromolecules as well as that of substances with nondirectional interactions that are capable of displaying liquid polymorphism.

DOI: 10.1103/PhysRevE.81.031201 PACS number(s): 61.20.−p, 61.25.−f, 64.70.D−

I. INTRODUCTION

Soft core potentials have a long history of being used to model isostructural critical points in crystals [1–4], polymorphism of crystal phases [5–7], liquid-liquid phase transitions (LLPTs) [6,8–15], polymorphism in glasses [16–19], and anomalous thermal expansion of liquids at low temperatures [6,9,10,17,20–29]. All these phenomena can be associated with the existence of two competing local structures: an expanded structure characterized by large open spaces between particles, and a collapsed structure in which particles are spaced more closely. The expanded structure is the result of quantum mechanical interactions between particles, interactions that differ depending upon the material. For example, in water the expanded structure is caused by four-coordinated hydrogen bonds that build a first coordination sphere of only four molecules [13,30–43], while in simple liquids, such as argon, the first coordination sphere consists of approximately twelve particles arranged in a closely packed configuration. Accordingly, water has much more empty space between molecules than argon and its density can be significantly increased by increasing the pressure which distorts the hydrogen bond structure and increases the number of particles in the first coordination sphere [21]. This distortion is associated with an increase in entropy and hence with a density anomaly (due to the Maxwell relation),

$$\alpha_P \equiv \frac{1}{V}\left(\frac{\partial V}{\partial T}\right)_P = -\frac{1}{V}\left(\frac{\partial S}{\partial P}\right)_T < 0, \tag{1}$$

where α_P is the thermal expansion coefficient.

The collapse of the open structure under pressure leads at low temperatures to two distinct glassy states: low-density amorphous solid and high-density amorphous solid, which transform into one another by pressurizing and depressurizing. This transformation between two glassy states is associated with hysteresis [16,19,44].

The interplay between two local structures at intermediate temperatures above the glass transition may lead under certain conditions to their spatial segregation and hence to a LLPT, the existence of which is hypothesized in water based on computer simulations [45] and the extrapolation of the heat capacity [46]. A direct observation of the LLPT has been made in yttrium aluminum garnet ($Y_3Al_5O_{12}$) [47,48]. The LLPT associated with the transformation from molecular to polymeric liquid has been theoretically predicted [49] and experimentally observed in liquid phosphorus [50,51].

There is a growing body of evidence, both experimental and computational, that LLPTs and polymorphic glasses may exist at high temperatures and pressures in group-IV elements like silicon [52–54] and germanium [55–58], certain molecular compounds such as silica (SiO_2) [59–61], ionic salts such as BeF_2 [62], but also in molten Al_2O_3-Y_2O_3 [47] and in triphenyl phosphite [63]. While some systems are characterized by weakly directional interactions [64], in triphenyl phosphite the dominating interaction is expected to be nondirectional, since the substance consists of a simple organic molecule with a small dipole moment and no tendency to form hydrogen bonds [65]. Hence it is possible that liquid polymorphism may also occur in materials characterized by nondirectional interactions. This possibility is supported by a recent observation of a transition between two amorphous polymorphs in $Ce_{55}Al_{45}$, a metallic glass with nondirectional bonds, in which the transition is caused by pressure-induced *f*-electron delocalization [66].

There is indirect experimental evidence for a LLPT in sulfur [67–69], selenium [70], and some molecular liquids [48,71,72]. *Ab initio* computer simulations suggest that LLPTs may exist in hydrogen [73–75] and nitrogen [76] at

high pressures and temperatures. Since the direct experimental observation of LLPT is often difficult, its existence can be hypothesized based on observation of other experimental features of the system which are usually associated with a LLPT, e.g., the melting line maximum, the presence of rich crystal polymorphism [21], the presence of density or diffusivity anomalies, or an increase in heat capacity or compressibility when cooled.

A LLPT can occur with or without anomalies, depending on the nature of the soft repulsion. In particular, it was found that for potentials with a hard core softened by a repulsive linear ramp [the hard core plus linear ramp (HCLR) potential] the LLPT is associated with anomalies [6], while the LLPT occurs without any anomalous behavior when the soft repulsion consists of a square shoulder [12,77–79]. The possibility that a LLPT may occur disjointed from anomalies was recently supported by the experimental study of triphenyl phosphite, where in association with the LLPT the heat capacity shows no anomalous behavior [63] and a density increase is expected upon cooling.

Liquid anomalies and polymorphism, although caused in different materials by different chemistry, have similar physics: namely all substances above have large open spaces between particles that collapse under pressure. Thus we need a tractable, universal model that can determine whether these features and phenomena are related or exist independently. The simplest model that satisfies these conditions is a spherically symmetric potential that has two distinct length scales: a soft core σ_1, which creates a low-density structure at low pressure, and a smaller hard core σ_0, which creates a high-density structure.

In principle, the hard core diameter σ_0 can approach zero, as in the Gaussian core potential [22]. These models with $\sigma_0 \to 0$ typically possess a rich crystalline polymorphism and, under certain conditions, exhibit liquid anomalies and re-entrant melting [negative slope of the melting line $T_{\mathrm{melt}}(P)$]. Since softening of strongly repulsive interactions through the addition of a soft repulsion proved essential to observe anomalous behavior, we focus here on the soft component of core-softened interactions. We investigate the relation between anomalies and melting behavior in systems where the interparticle interaction consists of only a finite soft repulsion. Specifically, we introduce a family of bounded repulsive interaction potentials obtained by cutting the linear ramp potential at different heights.

In the context of microscopic interactions of atomic systems, these bounded potentials are unphysical; the strong repulsion at short distances (related to the Pauli exclusion principle) always prevents full particle overlap in a true microscopic interaction. However, if one considers interactions among macromolecules, *effective* interactions may result in a bounded repulsion that allows the particles to "sit on top of each other," imposing only a finite energy cost for a full overlap [80,81].

In Sec. II we describe the model. In Sec. III we outline the simulation method used to map out the phase diagram. In Sec. IV we present our results and in Sec. V we discuss our conclusions.

II. SOFT CORE BOUNDED REPULSIVE INTERACTION POTENTIAL

Bounded repulsive potentials were proposed to model effective interactions in polymers, dendrimers, and microgels [80]. Two kinds of melting behavior have been reported for such potentials.

(a) Re-entrant melting, i.e., the melting line displays a local temperature maximum T_{max} in the temperature-pressure phase diagram, followed by a region where the melting line has a negative slope (as, e.g., in the Gaussian core model [22,82,83]). If one would increase the pressure of such a liquid, initially at a very low pressure and at a temperature slightly lower than T_{max}, then one would observe the liquid to first crystallize and then re-enter the liquid phase at higher pressure.

(b) Crystallization into a clustered solid at arbitrarily high temperatures, with a positively sloped melting line (as, e.g., in the penetrable sphere model [84]). In this case, the interaction varies slowly enough at small interparticle distances to allow for particles to overlap, thus giving rise to an effective attraction that promotes aggregation—the solid can always lower its free energy by allowing for multiply-occupied sites.

A criterion for such cluster formation was derived [85] on the basis of a mean field analysis, valid at large densities. If the Fourier transform $U(Q)$ of the interparticle potential is everywhere positive (called Q^+-type interactions in [85]) the system displays behavior (a), while if $U(Q)$ attains negative values (called $Q^{\pm}$-type interactions in [85]) the system displays behavior (b). The reason is that if $U(Q)$ has negative values, the mean field structure factor

$$S^{\mathrm{MFT}}(Q) = \frac{1}{1 + (\rho/T)U(Q)} \tag{2}$$

may diverge at any T for densities above $\rho_0 = -T/U(Q_0)$, where Q_0 is the value for which $U(Q)$ attains its negative minimum. Since $S(Q)$ can be interpreted as the density response function to an infinitesimal external field (on the basis of the fluctuation-dissipation theorem), a diverging value of $S(Q)$ signals an instability, and thus the system is expected to freeze at arbitrarily high temperatures, for all $\rho \geq \rho_0$. This means that the melting line has no temperature maximum, and therefore there is no re-entrant melting. As concerns waterlike anomalies, these have been found in the Gaussian core model [86,87], a typical Q^+-type system, while no anomalies were reported for $Q^{\pm}$-type systems such as the penetrable sphere model (PSM) [84] or the "generalized exponential model of index 4" (GEM-4) [88,89].

We consider here a family of bounded interactions obtained by cutting a repulsive linear ramp at different heights [Fig. 1(a)],

$$U(r) = \begin{cases} (1-\lambda)U_1, & \text{for } r \leq \sigma_{\mathrm{cut}} \\ (1 - r/\sigma_1)U_1, & \text{for } \sigma_{\mathrm{cut}} < r < \sigma_1 \\ 0, & \text{for } r \geq \sigma_1, \end{cases} \tag{3}$$

where $\lambda \equiv \sigma_{\mathrm{cut}}/\sigma_1$.

For $\lambda = 0$ the potential in Eq. (3) corresponds to the uncut repulsive linear ramp, whereas for $\lambda > 0$ it possesses a flat

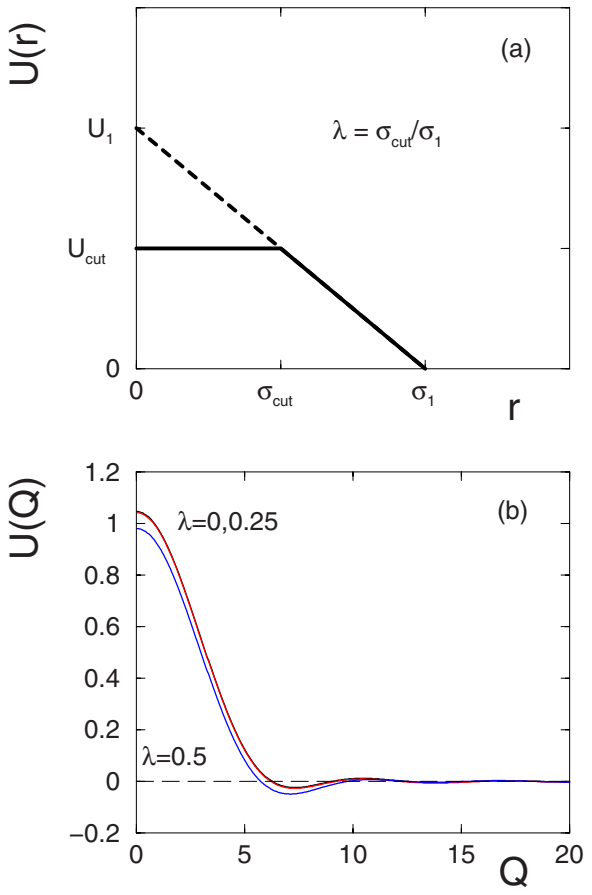

FIG. 1. (Color online) The family of potentials we introduce in this paper. (a) The cut ramp potential. For $\lambda \equiv \sigma_{cut}/\sigma_1 = 0$ the potential $U(r)$ corresponds to the uncut ramp potential, while for $\lambda \to 1$ it can be assimilated to the penetrable sphere interaction. (b) Fourier transform of the cut ramp potential for $\lambda = 0$, 0.25, and 0.5; the lines corresponding to $\lambda = 0$ and $\lambda = 0.25$ are indistinguishable on the scale of the figure.

region where the repulsive force vanishes for $r \leq \sigma_{cut}$. As λ increases the flat top gets larger and larger, and when $\lambda \to 1$ the potential approaches that of the penetrable sphere model [84]. All the potentials of the family described by Eq. (3) belong to the $Q^{\pm}$-type interaction class [Fig. 1(b)], so clustering is expected [behavior (b)], at sufficiently large particle densities.

III. METHODS

Throughout this paper we use reduced units in terms of length σ_1 and energy U_1. For temperature we use $T^* \equiv k_B T/U_1$, for pressure $P^* \equiv P\sigma_1^3/U_1$, and one time unit equals $\sigma_1\sqrt{m/U_1}$ seconds. Here k_B is the Boltzmann constant and m the mass of one particle.

For our simulations we use an implementation of the discrete molecular dynamics (DMD) algorithm. With DMD a continuous potential is approximated by a discrete potential made up of a series of steps [17,90,91]. For example, we approximate the potential of Eq. (3) by a series of small steps, each with length $\Delta r = 0.01\sigma_1$ and height $\Delta U = 0.01U_1$. The advantage of DMD is that it is event-driven and usually runs faster and/or is more stable than regular molecular dynamics (MD), especially at low densities. A regular MD simulation solves the equations of motion by numerical integration, which leads to numerical errors. In order to keep these errors as small as possible to prevent the system from becoming unstable, a small time step is to be used, causing the computer simulation to require more time.

In the case of a discrete potential $U(r)$ made up of steps $u_1, u_2, \ldots, u_n$, there is no need for numerical integration because a particle simply moves in a straight line with a constant velocity as long as r is such that $U(r)$ is constant. A "collision event" occurs when the distance r between two particles crosses one of the step boundaries. The main task in a DMD simulation is to calculate when the next collision occurs, and update the velocities of the particles involved after such an event. The new velocities are obtained from a simple calculation using the classical conservation laws for energy and momentum. For this reason DMD does not suffer from integration errors as the trajectories can be calculated to a precision bound only by the computer hardware. A drawback of the DMD algorithm is that it is more complex than basic MD. Furthermore, a lot of extra memory is needed to keep track of all the collision events. However, with modern day computers, the necessary memory has become less of a concern.

For all simulations with fixed particle number, constant volume, and constant temperature (NVT), we use the Berendsen thermostat to keep the system at a constant temperature, and for all NPT simulations an additional Berendsen barostat is used to keep the pressure constant. The implementation for DMD differs slightly from that for regular MD, but the algorithm [92] is the same. To keep the temperature near a value of T_0, we periodically calculate the kinetic temperature T of the system and then rescale the velocity of each particle by a factor of $[1+\kappa(T_0/T-1)]^{1/2}$. The thermal coefficient κ has a value between zero (thermally isolated system) and one (zero thermal resistance between the system and a heat reservoir at T_0). In regular MD the velocity is rescaled at fixed time intervals which are usually a multiple of the simulation time step Δt. Because DMD is event-driven there is no fixed time step, so we rescale the velocities after a certain number of collisions has occurred. In our simulations this number is always a multiple of N, the total number of particles in the system.

We follow a similar procedure for the Berendsen barostat in DMD. In this case we rescale the box size in order to keep the pressure constant. We allow the width, length, and height of the box to change independently of each other, using as parameters dx/dP_x, dy/dP_y, and dz/dP_z. To keep the pressure near a value of P_0 we calculate the average pressure of the system and then change the width by a factor of $1-(P_0 - P_x)\frac{dx}{dP_x}$. The length and height are rescaled in a similar fashion.

The system that we consider in our paper has a good heat conductance, and for this reason the type of thermostat has not been a main concern. Sometimes the Berendsen thermostat can lead to problems; one basically takes heat out of the entire system, and if the heat is produced in one particular place, e.g., on a crystal-liquid boundary, then this particular

place may obtain a higher temperature than the rest of the system, which can lead to artifacts. We have checked the temperature distribution of the system and found that it is in fact quite uniform and we observed no artifacts from the applied thermostat.

To explore the phase diagram of the family of potentials considered, we perform NVT simulations with 4000 particles in a cubic box of various sizes together with periodic boundary conditions. We first equilibrate each state point for a period of at least 700 time units, followed by a data taking period of about 2100 units of time. We use the Berendsen thermostat with a thermal coefficient of $\kappa=0.01$, and we rescale the velocity after every N collisions. After the trajectories of the particles are collected, we calculate the diffusion coefficient D, using

$$D = \lim_{t\to\infty} \frac{\langle [\mathbf{r}(t'+t) - \mathbf{r}(t')]^2 \rangle_{t'}}{6t}. \tag{4}$$

The notation $\langle \cdots \rangle_{t'}$ indicates an average taken over all particles and all time t', with $700 \le t' \le 2800$.

We analyze the melting line by performing simulations done at constant pressure and temperature (NPT). We locate the melting line by simulating a system that starts with one half being liquid and the other half being in the solid state. For each value of λ considered in this paper the crystal lattice is fcc, so the initial solid state is always chosen to be an fcc crystal. If at a given pressure P the crystal grows, then the temperature T lies below the melting temperature T_{melt}. But if the liquid grows, T must lie above T_{melt}. To prepare the initial state of half liquid/half solid, we first prepare an fcc crystal in the shape of a long box (its height twice as large as its width and length), containing 5600 particles with none of them overlapping. Since cluster formation is strongly related to the density, and thus the pressure, it is important to ensure that the fcc crystal has the number of clusters corresponding to the particular pressure P at which we are trying to find the melting temperature. This we accomplish by first melting half of the crystal at this pressure, and then making it recrystallize. Subsequently, we melt and recrystallize the other half. Additional local melting and recrystallization can be used to prevent grain boundaries from forming, to obtain a homogenous crystal with the correct amount of clustering. Localized melting can be done by replacing the interaction potential by a weaker potential, within a certain region of the box. Once the crystal has melted in this region, we restore the original potential. To ensure recrystallization, the initial state of half liquid/half solid must be prepared at a temperature slightly below T_{melt}.

After the crystal is placed at approximate thermal equilibrium with the liquid, with the liquid-crystal interface perpendicular to z axis, we perform production runs for several values of T in the vicinity of T_{melt}. Figure 2 shows the variations of the potential energy as a function of time. If the potential energy increases, the liquid grows, so $T > T_{\text{melt}}$. By extrapolating $U_{\text{pot}}(t)$ for different temperatures and looking at the slope of those curves, we are able to estimate the value of T_{melt} for a given pressure.

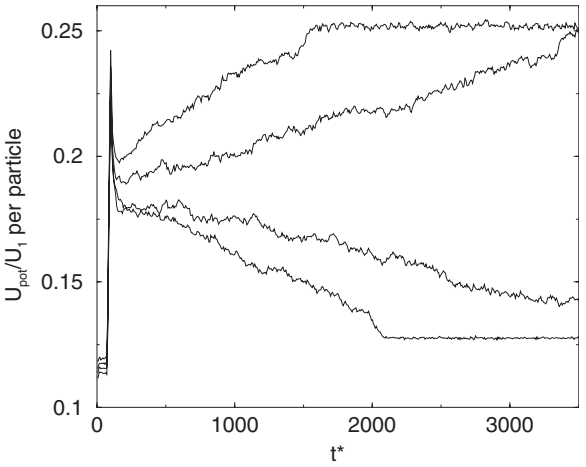

FIG. 2. Potential energy vs time, to help determine the melting temperature T^*_{melt} for the $\lambda=0$ cut at pressure $P^*=1.12$. Shown here is the potential energy $U_{\text{pot}}(t)$ for temperatures $T^*=0.0360, 0.0365, 0.0370, 0.0375$ (from bottom to top) for a box with 5600 particles, starting as an fcc crystal. After a short equilibration period, at $t^*=70$ half the crystal is melted by temporary lowering the interaction potential for the particles in the center of the box. At $t^*=100$ the interaction potential is restored and the simulation is allowed to run till $t^*=3500$. Considering the slope of $U_{\text{pot}}(t)$ one can determine if either the liquid or the crystal is growing. The lowest temperature (bottom graph) crystallizes completely before the simulation ends; the nearly constant potential energy indicates the system has reached equilibrium. Similarly, the system at the highest temperature is seen to liquefy completely near $t^*=1500$. The melting temperature at this pressure is estimated to be $T^*_{\text{melt}}=0.0367$.

For all simulations concerning the melting line, we set $\kappa=1$ for the Berendsen thermostat and perform velocity rescaling every N collisions. The volume is rescaled after every $10N$ collisions, with $dx/dP_x = dy/dP_y = 0$ and $dz/dP_z = 3.75 \times 10^{-4}$ (reduced units); i.e., the width and length of the box are fixed, and we only allow the height to vary. Simulations run for at least 3500 time units, and we apply periodic boundary conditions, as before.

IV. RESULTS

We calculate the liquid-solid coexistence line of a system of particles interacting through the potential defined in Eq. (3) for different values of λ (Fig. 3). Unlike the bounded potentials studied up to now, we find that for small λ the melting behavior of this model combines melting features typical of Q^+- and $Q^{\pm}$-type interactions. Let us consider the case $\lambda=0$, for example. At small pressures the melting line rises with a positive dT/dP slope, as one could expect, since in this dilute regime the potential is essentially impenetrable. As the pressure increases, the soft nature of the repulsion comes into play. The melting line bends and passes through a maximum in temperature, followed by a region with a negative slope where re-entrant melting occurs. In this region, the solid melts into a denser liquid when we increase the pressure at a constant temperature (Fig. 4). At higher pressure the slope recovers a positive value, and runs to higher tempera-

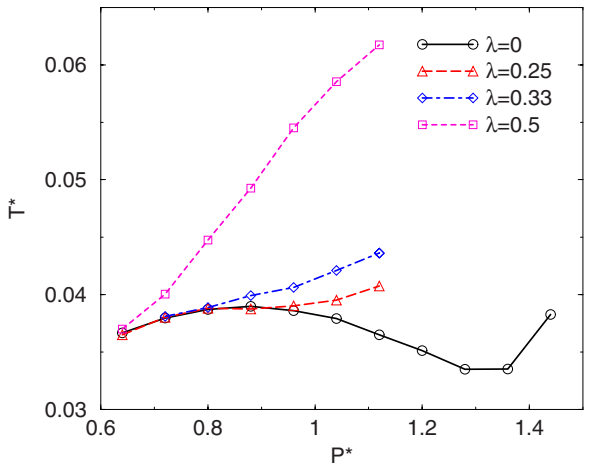

FIG. 3. (Color online) Liquid-solid melting line in the P-T plane for the cut ramp potential with $\lambda=0$, 0.25, 0.33, and 0.5. Axes are in reduced units: $P^*=P\sigma_1^3/U_1$ and $T^*=k_BT/U_1$. The region of anomalous re-entrant melting (a negative slope of the melting line) is clearly visible for $\lambda=0$.

tures and pressures. Given the bounded nature of the potential, the observed behavior suggests that at high pressures (where the melting line has positive dT/dP slope) the system crystallizes into a clustered solid.

For λ larger than $\lambda_c \approx 0.28$ the melting line has a positive dT/dP slope everywhere, a behavior similar to typical $Q^{\pm}$-type interactions such as the PSM or the GEM-4. The slope of the melting line becomes steeper and steeper as λ gets larger. In fact, as λ increases, the flat top of the potential becomes larger and larger, and the interparticle potential becomes increasingly similar to the penetrable sphere model interaction.

In order to relate melting behavior and cluster formation, we investigate the formation of aggregates of particles. As a measure to quantify clustering we adopt the average number $N_{\rm cl}$ of neighbors of a particle within a distance smaller than the first minimum r_0 (with $r_0 \leq \sigma_1$) of the radial distribution function (see Fig. 5)

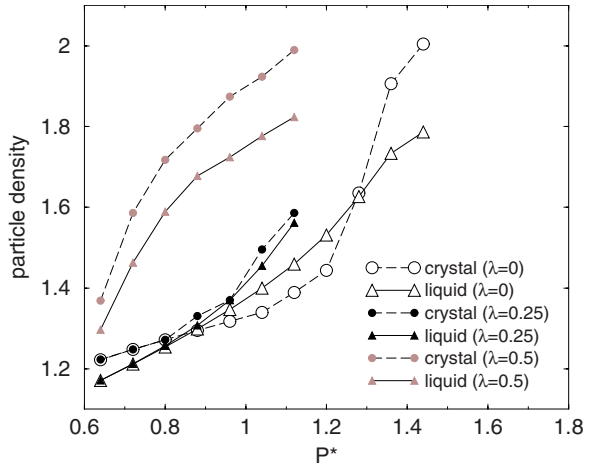

FIG. 4. (Color online) Particle density of the crystal and liquid on the melting line, for the cut ramp potential with $\lambda=0$, 0.25, and 0.5. For $\lambda=0$ and P^* roughly between 0.9 and 1.3 the liquid phase is denser than the coexisting solid.

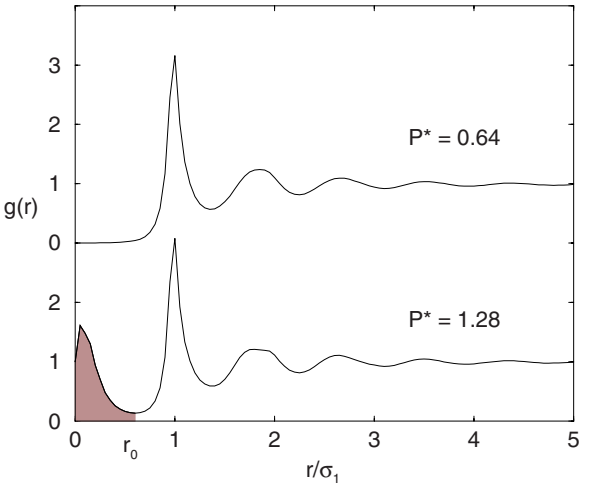

FIG. 5. (Color online) Explanation of how we determine the amount of clustering. Shown here is the radial distribution function $g(r)$ for the uncut ramp potential ($\lambda=\sigma_{\rm cut}/\sigma_1=0$). Both graphs refer to the liquid state at $T^*=0.035$. To quantify the amount of clustering, we calculate the average number of neighbors $N_{\rm cl}$ within a distance r_0, the first minimum of $g(r)$, i.e., $N_{\rm cl} \equiv \int_0^{r_0} 4\pi r^2 \rho g(r) dr$, where $r_0 \leq \sigma_1$. The corresponding region is indicated by the shaded area.

$$N_{\rm cl} \equiv \int_0^{r_0} 4\pi r^2 \rho g(r) dr, \tag{5}$$

where $\rho \equiv N/V$ is the particle density.

We calculate $N_{\rm cl}$ on the melting line for both the liquid and solid state, and show the results in Fig. 6. We find that at fixed pressure, $N_{\rm cl}$ depends sensitively on the value of λ, being larger for potentials with a wider flat top (large λ). This is consistent with the reduced repulsion around $r=0$ which favors the formation of clusters of particles. For a

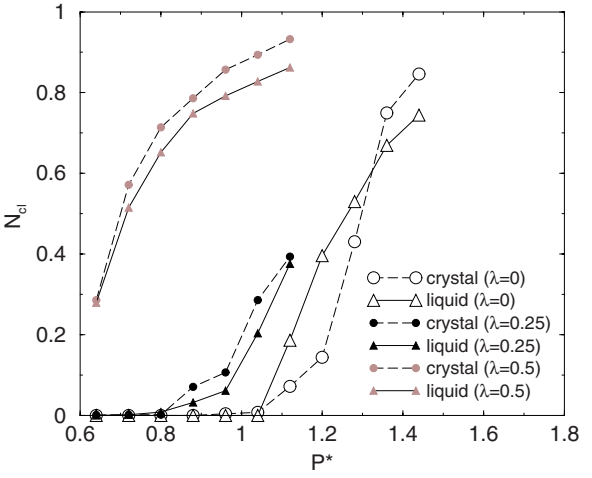

FIG. 6. (Color online) Average number of neighbors $N_{\rm cl}$ within a distance smaller than the first minimum of $g(r)$. Results are shown for temperatures on the melding line (both the liquid and solid state) for the cut ramp potential with $\lambda=0$, 0.25, and 0.5. In most cases the clustering is higher for the solid state, except for $\lambda=0$ in the pressure range corresponding to the anomalous region.

given λ, N_{cl} increases with the pressure, though the exact behavior depends on the value of λ. For small λ (i.e., $\lambda \leq \lambda_c$) no clustering occurs on the first portion of the melting line, and the phenomenon becomes important only when the melting slope becomes positive again after the local minimum in the melting line. For larger λ however, cluster formation is already significant at low pressures ($Q^{\pm}$-type interaction behavior) and N_{cl} attains large values rapidly. Values of N_{cl} close to one correspond to a system with double occupancy in which particles aggregate to form dimers. At high pressures N_{cl} may assume even larger values (especially for large λ) as more and more particles sit on top of each other. For a given λ, N_{cl} is generally larger in the solid state, with the exception of those regions where re-entrant melting occurs. This is particularly evident for $\lambda=0$, where in the pressure range corresponding to re-entrant melting, N_{cl} is larger in the liquid, which is denser than the coexisting solid (Fig. 4).

In general, the density (pressure) regime at which clustering sets in depends on the relative balance between the repulsive force around the particle core and that at $r=0$, which can be understood through the following qualitative argument. Consider a uniform arrangement of particles at densities just large enough so that the particles only begin to touch with each other. Moving two particles closer implies an energy cost (that is smaller as λ increases and the potential gets flatter), but at the same time, reducing the number of nearest neighbors yields an entropy gain, which gets larger as the average interparticle distance decreases. For large λ clustering is favored already at very low densities, whereas for small λ only at sufficiently large densities it is energetically convenient to move two particles closer such that cluster formation occurs.

The possibility of having the behavior of both Q^{+}-type systems and $Q^{\pm}$-type systems at the same time makes the cut ramp model particularly suited for exploring the relationship between melting, cluster formation, and waterlike anomalies. We find that this model exhibits both density and diffusion anomalies (Fig. 7). The region where the density anomaly occurs [delimited at high temperature by the temperature of maximum density (TMD) line] as well as the region of diffusion anomaly [delimited by the loci of diffusivity maxima and minima (DM)] are localized approximately in the same pressure range where re-entrant melting is found to occur. Another anomalous feature is the behavior of the isothermal compressibility, which increases upon cooling between the lines of maximal and minimal compressibility. The part of the low-density branch with a positive slope corresponds to the compressibility minima, while the high-density branch with $dP/dT>0$ and the low-density branch with $dP/dT<0$ correspond to the compressibility maxima. As in water and other liquids with a density anomaly, the isothermal compressibility line crosses the TMD line at both the point of its largest and its lowest temperature (there where the slope dP/dT is infinite), which is consistent with the mathematical properties of the second derivative of the equation of state [93]. As shown by the behavior of the isoclustering lines, the number of clusters increases with increasing the pressure at constant temperature. On the other hand, the amount of clustering decreases (though much less sensitively) upon increasing the temperature while keeping the pressure constant. The latter statement follows most clearly from Fig. 7 by noting that as one moves along a constant pressure path the isoclustering lines corresponding to lower and lower values of N_{cl} are successively crossed as T is increased. As λ increases, the isoclustering lines move toward lower pressures, as follows from the reduced repulsion at small r. At the same time, the anomalous region progressively shrinks and vanishes for λ just slightly larger than λ_c (Fig. 8), a phenomenon also observed in [29] for a different model.

A valuable insight into the relationship among waterlike anomalies, melting behavior, and cluster formation is provided by the analysis of the structural properties. Figure 9 shows a snapshot of a liquid/crystal system at $P^*=1.2$ and $T^*=0.35$ for the uncut ramp potential on the melting line. The fcc structure of the crystal is clearly visible and overlapping particles have been highlighted with a red color. To obtain a more quantitative analysis, we calculate for the uncut ramp potential ($\lambda=0$) the structure factor $S(Q)$ for several pressures at a constant temperature slightly larger than the maximum melting temperature $T^*_{max}\approx 0.039$. As shown in Fig. 10, with increasing pressure the system becomes at first more and more structured: all peaks go up while their position shifts slightly toward larger Q. This trend, related to the formation of the solid at low densities comes to a halt approximately at P_{max}, where P_{max} is the pressure corresponding to the maximum melting temperature T_{max}. Increasing the pressure further, brings us in the pressure range corresponding to re-entrant melting where $S(Q)$ remains essentially unaltered, both in the heights of the peaks and in their positions. This pressure range lies roughly between $P^*=0.8$ and 1.2, where $P^*\approx 1.2$ corresponds to the inflection point of the melting line. Finally, as we increase the pressure even further, we approach the high-density clustered solid and $S(Q)$ shows a remarkable increase of its first peak, and a less significant increase of the second one. For pressures where the liquid is supercooled (above $P^*\approx 1.45$ for $T^*=0.040$) the second peak also undergoes a topological modification, with a shoulder growing on top of it, while its position remains essentially unaltered.

This behavior is completely different from what has been reported up to now for bounded potentials that exhibit re-entrant melting. For example, in the GCM (a typical system with a Q^{+}-type interaction) as pressure increases in the range 0 to P_{max}, all peaks of $S(Q)$ go up, signaling that the system is undergoing an ordering process associated with the formation of the solid region at low densities. When the pressure increases further, all of the peaks decrease in height as the system becomes more and more disordered. With increasing P the positions of the peaks shift toward larger Q, which is consistent with closer spacing of particles resulting from the loss of efficacy of the soft core [83,87]. On the other hand, in typical systems that undergo clustering and where the melting line runs monotonically to high T and P (such as, e.g., the GEM-4 system, which can be considered the continuous analogous of the PSM), one finds that as P is isothermally increased, $S(Q)$ becomes more and more structured while the positions of the peaks remain unaltered. This is related to the crystallization of the liquid, where the system forms a lattice with a lattice constant that is independent of the density [89].

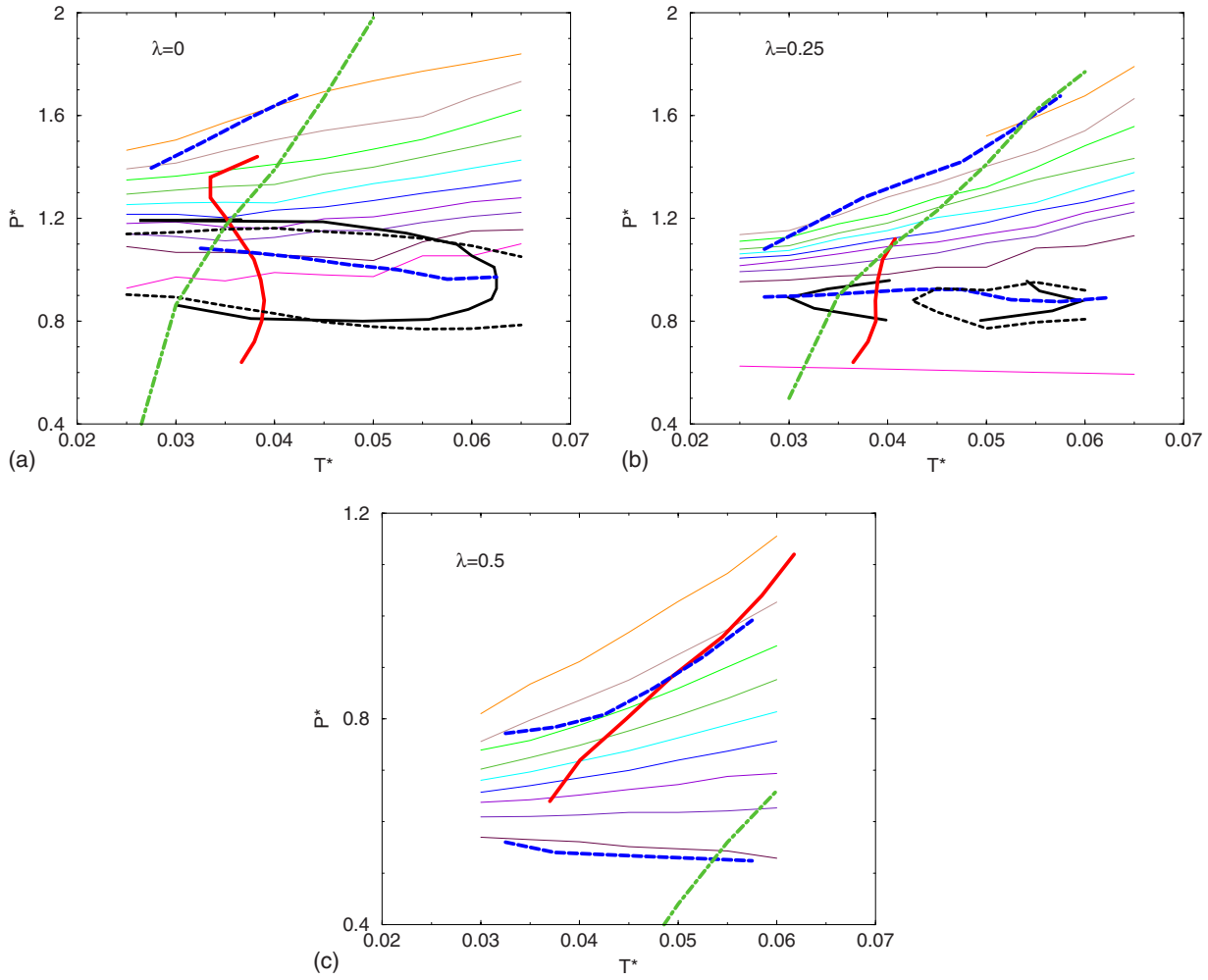

FIG. 7. (Color online) Phase diagram with isoclustering lines for the cut ramp potential with $\lambda=0$, 0.25, and 0.5. The isoclustering lines shown refer to the liquid phase (simulated deep into the supercooled liquid region), and run from $N_{cl}=0.9$ at the top (thin orange line) to $N_{cl}=0$ at the bottom (thin magenta line), in steps of 0.1. The line with $N_{cl}=0$ is omitted for $\lambda=0.5$. The thick solid red line is the melting line, which displays re-entrant melting where the slope dP/dT is negative. The black solid and black dashed lines are the TMD and DM lines, respectively. The loci of isothermal compressibility extrema are represented by the thick blue dashed line. The thick dot-dashed green line represents the mean-field instability line $\rho_0=-T/U(Q_0)$ above which the liquid becomes unstable and freezes, according to Eq. (2). The MFT instability line is exact in the limit of high density, so it is expected to be close to the melting line only at high pressures. In the case of $\lambda=0.5$ the pressures considered are lower than for the other values of λ, which explains the larger discrepancy. Axes are in reduced units: $P^*=P\sigma_1^3/U_1$ and $T^*=k_BT/U_1$.

In light of the above considerations, the results shown in Fig. 10 suggest that for the uncut ramp potential, clustering in the liquid phase plays already a role at intermediate densities, i.e., where re-entrant melting occurs. The insensitivity of $S(Q)$ to pressure in the liquid phase in the range corresponding to re-entrant melting (a feature never observed up to now for systems undergoing this kind of melting) can be understood by considering that in this region two contrasting effects come into play.

(i) On the one hand, there is the loss of efficacy of the soft core, which is associated with re-entrant melting. It causes the system to have the tendency to become more disordered, which shows in $S(Q)$ as a decrease of the peaks as well as a shift of the peaks toward higher Q.

(ii) On the other hand, with further increasing pressure the particles begin to overlap which causes $S(Q)$ to become more structured and, since the spacing of clusters is essentially density independent, the peak positions remains fixed. This is similar to what happens in $Q^{\pm}$-type interactions.

The independence of $S(Q)$ with respect to the pressure suggests that in the range of pressures corresponding to re-entrant melting the effects of the two mechanisms balance each other, at least as far as concerning the behavior of $S(Q)$. In re-entrant melting the low-density solid re-melts into a denser liquid. Usually the density increase with respect to the solid is due to a decrease of the average interparticle distance (related to the loss of efficacy of the repulsive length scale effective at smaller pressures). In the ramp potential however, the density increases because particles pile up to form clusters, while the cluster-cluster distance is essentially fixed—as is reflected by the fact that the peaks of $S(Q)$ do not show a shift toward higher Q. This behavior may be

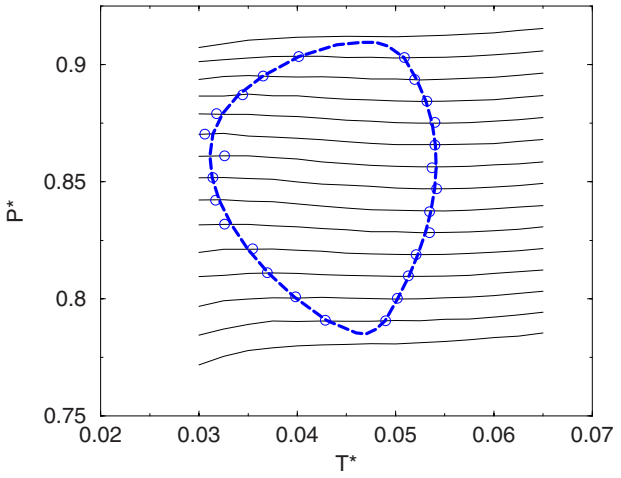

FIG. 8. (Color online) Density anomaly region for $\lambda_c=0.28$. Thin lines correspond to the isochores. The blue dashed line, drawn as a guide to the eye, indicates the temperature of minimum/maximum density (TMD). For λ slightly larger than λ_c, the anomalous region shrinks to a point and disappears. Axes are in reduced units: $P^*=P\sigma_1^3/U_1$ and $T^*=k_BT/U_1$.

considered as the fluid phase counterpart of the density-independent lattice constant that characterizes clustered solids.

As discussed above, the loss of efficacy of the soft length scale is balanced by the formation of particle clusters. This effect can be better appreciated by analyzing the radial distribution function $g(r)$ (see Fig. 11). At small pressures $g(r)$ has a peak at $r=\sigma_1$ and goes rapidly to zero for smaller interparticle distances, which means that in spite of its bounded nature, the repulsion is effective in keeping the particles apart. As P is increased, the peak at $r=\sigma_1$ grows and at the same time the values of $g(r)$ inside the soft core begin to grow, which signals that more and more particles start to fully overlap to form clusters. As the clustering process becomes significant (i.e., as the soft scale becomes less and less effective) the peak at $r=\sigma_1$ begins to decrease. This decrease occurs approximately in the range of pressures corresponding to re-entrant melting and the anomalous region. At the same time a new peak begins to develop inside the soft core, at $r/\sigma_1 \leq 0.1$. When the melting line acquires again a positive slope, the peak at $r=\sigma_1$ inverts its trend and begins to increase, while the peak at small r exhibits an extremely rapid growth and becomes larger and larger as the clustered solid is approached.

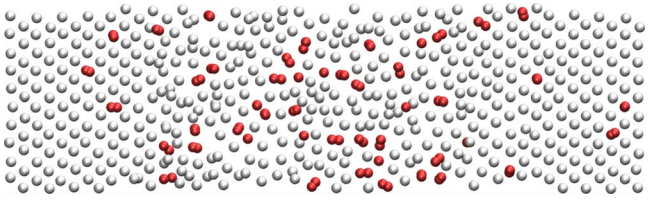

FIG. 9. (Color online) Snapshot of the liquid/crystal system for the uncut ramp potential ($\lambda=0$) at pressure $P^*=1.2$ and temperature $T^*=0.035$ (on the melting line). The complete system has a size of approximately $10\sigma_1\times10\sigma_1\times36\sigma_1$, but shown here is a thin slice of about one σ_1 thick. The fcc structure of the crystal is clearly visible at the ends, with the liquid phase in the center. The distance between two neighboring particles in the crystal is approximately one σ_1. Shown in red are the "clustered" particles (those that lie within a distance of $0.5\sigma_1$ of one other). This particular state point lies well within the anomalous region where the clustering N_{cl} inside the liquid is much higher than in the crystal (see also Fig. 6).

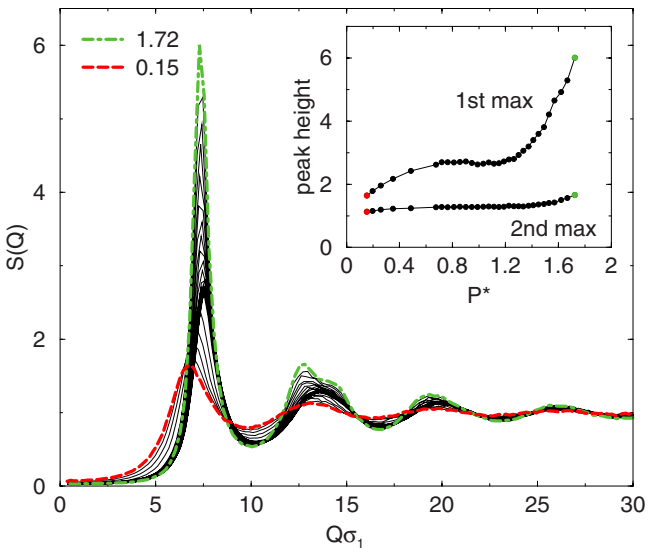

FIG. 10. (Color online) Structure factor $S(Q)$ of the uncut ramp potential ($\lambda=0$) at constant temperature ($T^*=0.040$) for several pressures, in steps of $\Delta P^*=0.0416$. The red dashed line represents $S(Q)$ for the smallest pressure ($P^*=0.15$), and the green dot-dashed line represents $S(Q)$ for the largest pressure ($P^*=1.72$). The apparent thick black line located between the red and green lines results from the overlap of many thin black lines in the range of pressures where $S(Q)$ changes very little with pressure. The range of densities considered in this figure is 0.75 to 2.05 particles/σ_1^3. Inset: Plot of peak heights of $S(Q)$ versus pressure, for the first and second maxima.

While the "explosion" of the peak at small r can easily be attributed to the particles overlapping, the increase of the peak at $r=\sigma_1$ may appear surprising at first, given that at such regimes the soft core has lost most of its efficacy. An explanation for this feature can be found in the nature of the clustering phenomenon itself. Complete or near-complete overlap of two particles is more convenient for the system than partial overlap of several particles, i.e., when several particles are at a distance from each other just smaller than the soft core. This restores part of the soft scale efficacy, and thus the height of the peak at $r=\sigma_1$ is found to increase. Essentially particles in the original system are replaced by closely aggregated dimers that interact with an effective potential twice as strong as the original potential. This is typical behavior for a $Q^{\pm}$ potential, where the soft scale efficacy in crystals is found to remain practically intact because of clustering, resulting in an essentially density-independent lattice constant [89].

With $g(r)$, the rise of a peak inside the soft core is a clear indication of the interpenetration of the particles followed by the formation of clusters. However, we observe in the uncut ramp liquid a feature not found in other fluids that undergo clustering (such as PSM or GEM-4): the development of

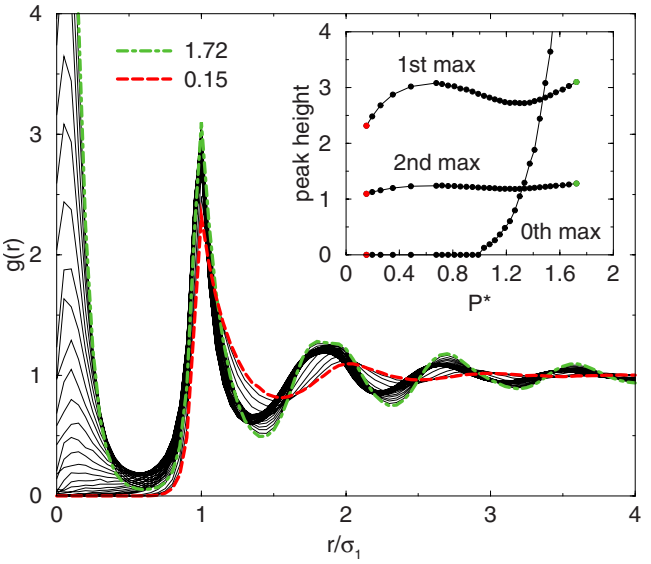

FIG. 11. (Color online) Radial distribution function of the uncut ramp potential ($\lambda=0$) at constant temperature ($T^*=0.040$) for several pressures, in steps of $\Delta P^*=0.0416$. The red dashed line represents $g(r)$ for the smallest pressure ($P^*=0.15$), and the green dot-dashed line represents $g(r)$ for the largest pressure ($P^*=1.72$). The apparent thick black line located between the red and green lines results from the overlap of many thin black lines in the range of pressures where $g(r)$ changes very little with pressure. Inset: Plot of the peak heights of $g(r)$ versus pressure, for the first and second maximum, as well as the "zeroth" maximum which is the peak at $r<\sigma_1$.

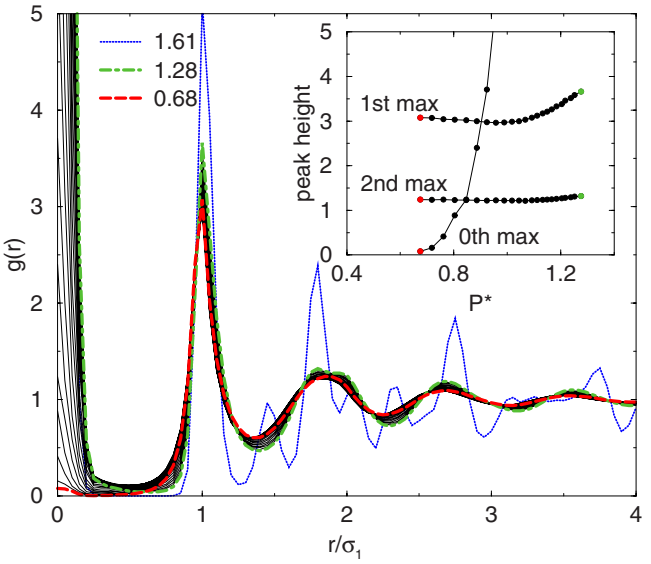

FIG. 12. (Color online) Radial distribution function of the cut ramp potential ($\lambda=0.25$) at constant temperature ($T^*=0.040$) for several pressures. The red dashed line represents $g(r)$ for the smallest pressure ($P^*=0.68$), and the green dot-dashed line represents $g(r)$ for the largest pressure for which the system remains liquid ($P^*=1.28$). As a comparison, we have included the $g(r)$ of the system at pressure $P^*=1.61$ (thin blue dotted line), which spontaneously crystallizes into an FCC structure. Inset: Plot of the peak heights of $g(r)$ versus pressure, for the first and second maximum, as well as the "zeroth" maximum which is the peak at $r=0$.

such a peak at a nonzero distance. According to this feature, though complete overlapping is highly probable at high pressure, the most probable arrangement is one in which particles partially overlap with their centers separated by a distance of the order of $0.1\sigma_1$. This is due to the presence in the ramp potential of a repulsive force acting also at $r=0$, whereas in the PSM or GEM-4 systems the repulsion vanishes at $r=0$. It is reasonable to assume that as pressure gets higher and higher, the position of the main peak of $g(r)$ will move closer to zero. Unlike the uncut ramp potential, the cut ramp potential ($\lambda>0$) has no repulsive force at $r=0$ and one may therefore expect a peak growing at zero distance. This is indeed the case, as is shown in Fig. 12 for $\lambda=0.25$.

The results that we have obtained illustrate for our system the close relationship between waterlike anomalies and the soft nature of the repulsive length scale. At pressures sufficiently high such that the soft length scale loses its efficacy [as shown by the decrease of the peak of $g(r)$ corresponding to the soft radius, and the rise of a new peak inside the core], anomalous structural and thermodynamical behavior occur, as well as re-entrant melting. At even higher pressures, where the formation of clusters becomes dominant, clustering gives rise to an essentially persistent effective length scale [reflected in the increase of the peak of $g(r)$ at $r=\sigma_1$], thus "undermining" a basic condition for the onset of anomalies.

We finally investigate the behavior of a system of particles interacting through a potential that consists of an impenetrable hard core surrounded by a soft core, where the soft core is again a linear ramp [5],

$$U(r)=\begin{cases}\infty, & \text{for } r\le\sigma_0\\ (1-r/\sigma_1)U_1, & \text{for } \sigma_0<r<\sigma_1\\ 0, & \text{for } r\ge\sigma_1.\end{cases} \tag{6}$$

It has been shown that the HCLR potential (Fig. 13) can display waterlike anomalies, provided that the ratio Λ between the hard core radius, σ_0, and the total interaction range, σ_1, is not too large [27]. We choose $\Lambda=4/7$ (for which anomalous behavior was reported [17]) and analyze the relationship among the melting line, the anomalous behavior, and the structural properties.

As shown in Fig. 13, the melting line displays a positive dT/dP slope at small pressures, consistent with the substantial impenetrability of the soft ramp in the dilute regime. As pressure increases, the soft repulsive ramp becomes less and less effective and the melting line passes through a maximum in temperature, followed by a region where re-entrant melting occurs. As expected, in this small-intermediate pressure range the melting line of the HCLR almost overlaps with that of the ramp potential, since the presence of the hard core is "screened" by the soft repulsion. At higher pressures, where the soft repulsion becomes ineffective, the HCLR potential is characterized by the hard core repulsion, and the melting line accordingly recovers a positive slope. At these high pressures the liquid crystallizes into a rhombohedral lattice [17], while in models with a bounded potential clustering results in a complete overlap and the system crystallizes into a fcc structure with multiple occupancy. The density and diffusion anomalies occur in the pressure range

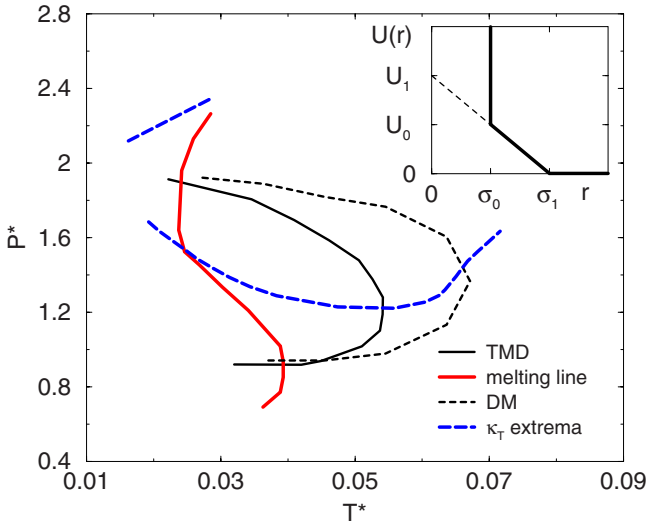

FIG. 13. (Color online) Phase diagram of the hard core plus linear ramp (HCLR) potential. Solid red line indicates the melting line. The black solid line and dashed lines are the temperature at maximum/minimum density (TMD) and the diffusion extrema (DM) lines, respectively. The thick blue dashed lines represents the loci of compressibility extrema. Axes are in reduced units: $P^* = P\sigma_1^3/U_1$ and $T^* = k_B T/U_1$. Inset: The hard core plus linear ramp potential $U(r)$ as a function of the interparticle distance r.

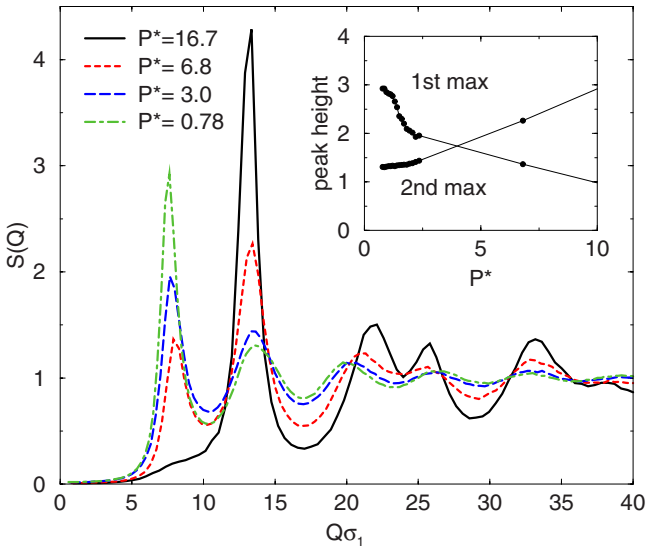

FIG. 14. (Color online) Structure factor of the hard core plus linear ramp potential at constant temperature ($T^*=0.036$) for several pressures. The first peak of $S(Q)$ decreases with increasing pressure, and at pressures below $P^* \approx 4$ the first peak of $S(Q)$ is the largest, while the second peak is the largest above $P^* \approx 4$. In fact, at very high pressures the first peak is found to disappear completely. Inset: Plot of peak heights of $S(Q)$ versus pressure, for the first and second maxima.

where the HCLR system undergoes re-entrant melting, while both anomalies are found to disappear at higher pressures where the melting line recovers a positive slope.

As can be appreciated by comparing Figs. 7 and 13, the phase diagram of the HCLR potential has a similar topology as that of the ramp potential. However, the physical mechanism that cause such apparently similar behavior, present some remarkable differences. While the bounded ramp potential is characterized by just one length scale, the HCLR interaction possesses two repulsive length scales—the soft core (effective at low P,T) and the hard core (effective at high P,T). The turning on and off of the efficacy of these two length scales, is made evident by the analysis of the structure factor (see Fig. 14). As pressure increases, the first peak of $S(Q)$ initially increases. This peak is associated with the larger soft radius, and its increase is in correspondence with the formation of the solid at low density. As the pressure is increased further, the peak decreases as the soft scale loses its efficacy and the low-density solid re-melts. At intermediate and high pressures the second peak (related to the hard length scale) increases more and more, which signals the formation of a high-density solid similar to the crystal of hard spheres. Thus the mechanism giving rise to the phase behavior of the HCLR system is essentially based on the presence of two length scales and on the alternation of their efficacy with pressure.

A common feature of the linear ramp and HCLR potentials is that in both systems re-entrant melting and anomalous behavior can be related to the loss of efficacy of the soft scale at intermediate densities. However, the positive dT/dP slope of the melting line at high densities have completely different origins. In the linear ramp it arises from the dominance of the clustering phenomenon that at such regimes "forces" the efficacy of the soft scale, as shown by the increase of the first peak of $S(Q)$: while the soft repulsion is completely ineffective for particles within each cluster, the net cluster-cluster interaction still possess a significant soft core, keeping the cluster-cluster separation essentially density-independent. On the other hand, in the HCLR potential [where the first peak of $S(Q)$ disappears] the positive slope of the melting line at high densities is the result of the presence of an inner hard core.

The presence of a soft repulsive component in addition to a hard core may give rise to cluster formation in core-softened interactions, provided that the hard radius is sufficiently small with respect to the soft one. For instance, the phenomenon of cluster formation has also been observed in the hard core plus square shoulder (HCSS) potential [94–96], and is found to be robust upon the introduction of an attractive component of the interaction [97]. Cluster morphology in core-softened interactions like the HCSS is considerably more complex than is the case for bounded potentials, since a full overlap is explicitly forbidden when there is a hard core. Accordingly, for these types of potentials the effects of cluster formation on the phase behavior can be expected to be less relevant than for the bounded potentials, due to the dominance of the hard core repulsion at high pressures.

V. DISCUSSION AND CONCLUSIONS

In conclusion, we show that the two phenomena of (a) re-entrant melting and (b) crystallizing into a clustered solid can be observed (at different pressures) in the same system, this system is described by the repulsive linear ramp poten-

tial or by a linear ramp potential cut at not too low heights. Previously, these two phenomena have not been observed together in the same system. For the cut ramp model, we observe a full spectrum of waterlike anomalies in the pressure range corresponding to the re-entrant melting. The anomalous behavior tends to disappear as the ramp is cut at lower and lower heights, thus becoming more and more similar to the penetrable sphere interaction ($\lambda \to 1$). We find the critical value for λ to be $\lambda_c \approx 0.28$; we observe anomalous behavior for the cut ramp potential with $\lambda < \lambda_c$, while observing none for values of λ larger than λ_c.

To relate formation of clusters of particles with the melting behavior of the liquid, we introduce the clustering parameter N_{cl}, defined in Eq. (5), as the average number of neighbors of a particle within a distance smaller than the first minimum of $g(r)$. The amount of clustering N_{cl} depends heavily on the pressure and the value of λ. As the pressure is increased, N_{cl} rises, and the same happens when the ramp is cut to lower heights (i.e., increasing λ).

The clustering N_{cl} shows anomalous behavior on the melting line, which is related to re-entrant melting. The "clustering anomaly" is characterized by having a higher amount of clustering in the liquid state than in the solid state, and is most clearly visible for $\lambda = 0$ in Fig. 6. Re-entrant melting means that there exists a range of pressures for which the melting line has a negative slope $dT/dP < 0$. The Clapeyron equation then tells us that

$$\frac{dP}{dT} = \frac{S_{\mathrm{liquid}} - S_{\mathrm{solid}}}{V_{\mathrm{liquid}} - V_{\mathrm{solid}}} < 0, \tag{7}$$

and since the solid state has a higher degree of order than the liquid state, $S_{\mathrm{liquid}} > S_{\mathrm{solid}}$, we thus conclude that in exactly the same pressure range $V_{\mathrm{liquid}} < V_{\mathrm{solid}}$, i.e., the particle density of the liquid is higher than that of the solid. Comparing Figs. 3 and 4 for $\lambda = 0$, we see that both anomalies indeed occur in the same pressure range, namely $0.9 < P^* < 1.3$ approximately.

Within this pressure range there is less volume per particle available in the liquid, than in the solid state. Evidently, it is therefore to be expected that the amount of clustering is larger in the liquid state for these pressures, simply because there is less space available. However, this qualitative statement to explain the clustering anomaly ignores the way the particles are distributed over the available volume, and therefore fails at low densities where N_{cl} is small. We refer to the case of $\lambda = 0$ in Fig. 4 and 6, which indicate that both anomalies disappear at pressures above $P^* \approx 1.3$. On the other hand, the density anomaly does not exist for pressures below $P^* \approx 0.9$, while the clustering anomaly already disappears at pressures below $P^* \approx 1.05$ (where N_{cl} vanishes for the liquid state).

In the range of pressures where re-entrant melting occurs, the structure factor of the uncut linear ramp potential is more or less insensitive to pressure (both in the heights of the peaks and in their positions), a feature never reported in association with re-entrant melting. This behavior is related to the formation of clusters of particles, which balances the tendency of $S(Q)$ to get less structured in the pressure range where re-entrant melting occurs. However, a detailed analysis based on the study of the radial distribution function $g(r)$ makes evident that in the region where re-entrant melting and waterlike anomalies occur, the soft length scale loses its efficacy because of the pressure increase. The clustering phenomenon eventually restores the soft scale efficacy by enforcing an approximately constant distance between the clusters. Thus the onset of clustering weakens and eventually overturns the very physical basis of anomalies.

Though we considered here a simplified model system, our results may be useful to better understand the phase behavior of macromolecules as well as that of substances with nondirectional interactions able to show liquid polymorphism [63,66].

ACKNOWLEDGMENTS

We wish to thank C. A. Angell, M. C. Barbosa, G. Franzese, S. Han, Y. Katayama, P. Kumar, C. N. Likos, J. Luo, P. F. McMillan, E. Strekalova, and Hajime Tanaka for fruitful discussions, and the NSF Chemistry Division for support. S.V.B. thanks the Office of the Academic Affairs of Yeshiva University for funding the Yeshiva University high-performance computer cluster, and acknowledges the partial support of this research through the Dr. Bernard W. Gamson Computational Science Center at Yeshiva College.

[1] P. C. Hemmer and G. Stell, Phys. Rev. Lett. **24**, 1284 (1970).
[2] G. Stell and P. C. Hemmer, J. Chem. Phys. **56**, 4274 (1972).
[3] D. A. Young and B. J. Alder, Phys. Rev. Lett. **38**, 1213 (1977).
[4] E. Velasco, L. Mederos, G. Navascues, P. C. Hemmer, and G. Stell, Phys. Rev. Lett. **85**, 122 (2000).
[5] E. A. Jagla, Phys. Rev. E **58**, 1478 (1998).
[6] E. A. Jagla, J. Chem. Phys. **111**, 8980 (1999).
[7] P. J. Camp, Phys. Rev. E **68**, 061506 (2003); **71**, 031507 (2005).
[8] P. G. Debenedetti and H. E. Stanley, Phys. Today **56**(6), 40 (2003).
[9] P. G. Debenedetti, V. S. Raghavan, and S. S. Borick, J. Phys. Chem. **95**, 4540 (1991).
[10] M. R. Sadr-Lahijany, A. Scala, S. V. Buldyrev, and H. E. Stanley, Phys. Rev. Lett. **81**, 4895 (1998).
[11] E. A. Jagla, Phys. Rev. E **63**, 061501 (2001).
[12] G. Franzese, G. Malescio, A. Skibinsky, S. V. Buldyrev, and H. E. Stanley, Nature (London) **409**, 692 (2001).
[13] S. V. Buldyrev *et al.*, Physica A **304**, 23 (2002).
[14] S. V. Buldyrev and H. E. Stanley, Physica A **330**, 124 (2003).
[15] H. M. Gibson and N. B. Wilding, Phys. Rev. E **73**, 061507 (2006).
[16] E. A. Jagla, Phys. Rev. E **63**, 061509 (2001).
[17] P. Kumar, S. V. Buldyrev, F. Sciortino, E. Zaccarelli, and H. E.

Stanley, Phys. Rev. E **72**, 021501 (2005).
[18] L. Xu *et al.*, Proc. Natl. Acad. Sci. U.S.A. **102**, 16558 (2005); L. Xu, S. V. Buldyrev, C. A. Angell, and H. E. Stanley, Phys. Rev. E **74**, 031108 (2006).
[19] L. Xu, S. V. Buldyrev, N. Giovambattista, C. A. Angell, and H. E. Stanley, J. Chem. Phys. **130**, 054505 (2009).
[20] C. H. Cho, S. Singh, and G. W. Robinson, Phys. Rev. Lett. **76**, 1651 (1996).
[21] C. H. Cho, S. Singh, and G. W. Robinson, Faraday Discuss. **103**, 19 (1996).
[22] F. H. Stillinger and D. K. Stillinger, Physica A **244**, 358 (1997).
[23] M. R. Sadr-Lahijany, A. Scala, S. V. Buldyrev, and H. E. Stanley, Phys. Rev. E **60**, 6714 (1999); A. Scala, M. R. Sadr-Lahijany, N. Giovambattista, S. V. Buldyrev, and H. E. Stanley, *ibid.* **63**, 041202 (2001).
[24] N. B. Wilding and J. E. Magee, Phys. Rev. E **66**, 031509 (2002).
[25] Z. Yan, S. V. Buldyrev, N. Giovambattista, and H. E. Stanley, Phys. Rev. Lett. **95**, 130604 (2005).
[26] P. A. Netz, S. V. Buldyrev, M. C. Barbosa, and H. E. Stanley, Phys. Rev. E **73**, 061504 (2006).
[27] Z. Yan, S. V. Buldyrev, N. Giovambattista, P. G. Debenedetti, and H. E. Stanley, Phys. Rev. E **73**, 051204 (2006).
[28] Z. Yan, S. V. Buldyrev, P. Kumar, N. Giovambattista, P. G. Debenedetti, and H. E. Stanley, Phys. Rev. E **76**, 051201 (2007); Z. Yan, S. V. Buldyrev, and H. E. Stanley, *ibid.* **78**, 051201 (2008).
[29] A. B. de Oliveira, P. A. Netz, and M. C. Barbosa, EPL **85**, 36001 (2009).
[30] L. Bosio, S. H. Chen, and J. Teixeira, Phys. Rev. A **27**, 1468 (1983).
[31] F. Sciortino, A. Geiger, and H. E. Stanley, Phys. Rev. Lett. **65**, 3452 (1990); Nature (London) **354**, 218 (1991).
[32] M. Canpolat *et al.*, Chem. Phys. Lett. **294**, 9 (1998).
[33] E. Schwegler, G. Galli, and F. Gygi, Phys. Rev. Lett. **84**, 2429 (2000).
[34] A. K. Soper and M. A. Ricci, Phys. Rev. Lett. **84**, 2881 (2000).
[35] A. Botti, F. Bruni, A. Isopo, M. A. Ricci, and A. K. Soper, J. Chem. Phys. **117**, 6196 (2002).
[36] A. M. Saitta and F. Datchi, Phys. Rev. E **67**, 020201(R) (2003).
[37] Th. Strässle, A. M. Saitta, Y. Le Godec, G. Hamel, S. Klotz, J. S. Loveday, and R. J. Nelmes, Phys. Rev. Lett. **96**, 067801 (2006).
[38] Z. Yan, S. V. Buldyrev, P. Kumar, N. Giovambattista, and H. E. Stanley, Phys. Rev. E **77**, 042201 (2008).
[39] F. Mallamace *et al.*, Proc. Natl. Acad. Sci. U.S.A. **104**, 424 (2007).
[40] D. Paschek, Phys. Rev. Lett. **94**, 217802 (2005).
[41] P. H. Poole, I. Saika-Voivod, and F. Sciortino, J. Phys.: Condens. Matter **17**, L431 (2005).
[42] M. Yamada, S. Mossa, H. E. Stanley, and F. Sciortino, Phys. Rev. Lett. **88**, 195701 (2002).
[43] L. Xu *et al.*, Nat. Phys. **5**, 565 (2009).
[44] O. Mishima, L. D. Calvert, and E. Whalley, Nature (London) **314**, 76 (1985).
[45] P. H. Poole, F. Sciortino, U. Essmann, and H. E. Stanley, Nature (London) **360**, 324 (1992).
[46] C. A. Angell, Annu. Rev. Phys. Chem. **34**, 593 (1983); Phys. Chem. Chem. Phys. **2**, 1559 (2000).
[47] S. Aasland and P. F. McMillan, Nature (London) **369**, 633 (1994).
[48] M. C. Wilding, M. Wilson, and P. F. McMillan, Chem. Soc. Rev. **35**, 964 (2006).
[49] D. Hohl and R. O. Jones, Phys. Rev. B **50**, 17047 (1994).
[50] Y. Katayama, J. Non-Cryst. Solids **312-314**, 8 (2002).
[51] Y. Katayama *et al.*, Nature (London) **403**, 170 (2000); Science **306**, 848 (2004).
[52] S. Sastry and C. A. Angell, Nature Mater. **2**, 739 (2003).
[53] T. Morishita, Phys. Rev. Lett. **93**, 055503 (2004).
[54] P. F. McMillan, Nature Mater. **4**, 680 (2005); J. Mater. Chem. **14**, 1506 (2004).
[55] E. Rapoport, J. Chem. Phys. **48**, 1433 (1968).
[56] H. Bhat *et al.*, Nature (London) **448**, 787 (2007).
[57] V. Molinero and E. B. Moore, J. Phys. Chem. B **113**, 4008 (2009).
[58] V. Molinero, S. Sastry, and C. A. Angell, Phys. Rev. Lett. **97**, 075701 (2006).
[59] C. Meade, R. J. Hemley, and H. K. Mao, Phys. Rev. Lett. **69**, 1387 (1992).
[60] P. H. Poole, M. Hemmati, and C. A. Angell, Phys. Rev. Lett. **79**, 2281 (1997).
[61] I. Saika-Voivod, P. H. Poole, and F. Sciortino, Nature (London) **412**, 514 (2001); I. Saika-Voivod, F. Sciortino, and P. H. Poole, Phys. Rev. E **63**, 011202 (2000).
[62] M. Hemmati, C. T. Moynihan, and C. A. Angell, J. Chem. Phys. **115**, 6663 (2001).
[63] H. Tanaka, R. Kurita, and H. Mataki, Phys. Rev. Lett. **92**, 025701 (2004); R. Kurita and H. Tanaka, Science **306**, 845 (2004).
[64] M. Wilson and P. F. McMillan, Phys. Rev. B **69**, 054206 (2004); P. A. Madden and M. Wilson, J. Phys.: Condens. Matter **12**, A95 (2000).
[65] J. Senker and E. Rössler, Chem. Geol. **174**, 143 (2001).
[66] H. W. Sheng *et al.*, Nature Mater. **6**, 192 (2007).
[67] V. V. Brazhkin, R. N. Voloshin, S. V. Popova and A. G. Umnov, J. Phys.: Condens. Matter **4**, 1419 (1992).
[68] J. S. Tse and D. D. Klug, Phys. Rev. B **59**, 34 (1999).
[69] G. G. N. Angilella, F. E. Leys, N. H. March, and R. Pucci, Phys. Chem. Liq. **41**, 211 (2003).
[70] Y. Katayama, J. Synchrotron Radiat. **8**, 182 (2001).
[71] R. Kurita and H. Tanaka, J. Phys.: Condens. Matter **17**, L293 (2005).
[72] F. Sciortino, J. Phys.: Condens. Matter **17**, V7 (2005).
[73] O. Pfaffenzeller and D. Hohl, J. Phys.: Cond. Matter **9**, 11023 (1997).
[74] S. Scandolo, Proc. Natl. Acad. Sci. U.S.A. **100**, 3051 (2003).
[75] S. A. Bonev, E. Schwegler, T. Ogitsu, and G. Galli, Nature (London) **431**, 669 (2004).
[76] B. Boates and S. A. Bonev, Phys. Rev. Lett. **102**, 015701 (2009).
[77] G. Franzese, G. Malescio, A. Skibinsky, S. V. Buldyrev, and H. E. Stanley, Phys. Rev. E **66**, 051206 (2002); G. Malescio *et al.*, J. Phys.: Condens. Matter **14**, 2193 (2002); A. Skibinsky, S. V. Buldyrev, G. Franzese, G. Malescio, and H. E. Stanley, Phys. Rev. E **69**, 061206 (2004); G. Malescio, G. Franzese, A. Skibinsky, S. V. Buldyrev, and H. E. Stanley, *ibid.* **71**, 061504 (2005).
[78] N. M. Barraz, E. Salcedo, and M. C. Barbosa, J. Chem. Phys.

131, 094504 (2009).
[79] M. Sperl *et al.*, Phys. Rev. Lett. (to be published).
[80] C. N. Likos, Phys. Rep. **348**, 267 (2001).
[81] F. W. Starr and F. Sciortino, J. Phys.: Condens. Matter **18**, L347 (2006); C. W. Hsu and F. W. Starr, Phys. Rev. E **79**, 041502 (2009); C. W. Hsu *et al.*, Proc. Natl. Acad. Sci. U.S.A. **105**, 13711 (2008).
[82] F. H. Stillinger, J. Chem. Phys. **65**, 3968 (1976).
[83] A. Lang, C. N. Likos, M. Watzlawek, and H. Löwen, J. Phys.: Condens. Matter **12**, 5087 (2000); S. Prestipino, F. Saija, and P. V. Giaquinta, Phys. Rev. E **71**, 050102(R) (2005).
[84] C. N. Likos, M. Watzlawek, and H. Löwen, Phys. Rev. E **58**, 3135 (1998).
[85] C. N. Likos, A. Lang, M. Watzlawek, and H. Löwen, Phys. Rev. E **63**, 031206 (2001).
[86] W. P. Krekelberg, T. Kumar, J. Mittal, J. R. Errington, and T. M. Truskett, Phys. Rev. E **79**, 031203 (2009).
[87] P. Mausbach and H. O. May, Fluid Phase Equilib. **249**, 17 (2006).
[88] B. M. Mladek, D. Gottwald, G. Kahl, M. Neumann, and C. N. Likos, Phys. Rev. Lett. **96**, 045701 (2006).
[89] C. N. Likos *et al.*, J. Chem. Phys. **126**, 224502 (2007).
[90] D. C. Rapaport, *The Art of Molecular Dynamic Simulation* (Cambridge University Press, Cambridge, 1995).
[91] S. V. Buldyrev, in *Aspects of Physical Biology*, Lecture Notes in Physics, edited by G. Franzese and M. Rubi (Springer-Verlag, Berlin, 2008), pp. 97–131.
[92] H. J. C. Berendsen, J. Chem. Phys. **81**, 3684 (1984).
[93] S. Sastry, P. G. Debenedetti, F. Sciortino, and H. E. Stanley, Phys. Rev. E **53**, 6144 (1996).
[94] G. Malescio and G. Pellicane, Nature Mater. **2**, 97 (2003).
[95] M. A. Glaser *et al.*, EPL **78**, 46004 (2007).
[96] G. Malescio, J. Phys.: Condens. Matter **19**, 073101 (2007).
[97] G. Malescio and G. Pellicane, Phys. Rev. E **70**, 021202 (2004).